

Bulk flows and CMB dipole anisotropy in cosmological void models

Kenji Tomita

Yukawa Institute for Theoretical Physics, Kyoto University, Kyoto 606-8502, Japan

tomita@yukawa.kyoto-u.ac.jp

ABSTRACT

The observational behavior of spherically symmetric inhomogeneous cosmological models is studied, which consist of inner and outer homogeneous regions connected by a shell or an intermediate self-similar region. It is assumed that the present matter density parameter in the inner region is smaller than that in the outer region, and the present Hubble parameter in the inner region is larger than that in the outer region. Then galaxies in the inner void-like region can be seen to have a bulk motion relative to matter in the outer region, when we observe them at a point O deviated from the center C of the inner region. Their velocity v_p in the CD direction is equal to the difference of two Hubble parameters multiplied by the distance between C and O. It is found also that the velocity v_d corresponding to CMB dipole anisotropy observed at O is by a factor ≈ 10 small compared with v_p . This behavior of v_d and v_p may explain the puzzling situation of the cosmic flow of cluster galaxies, when the radius of the inner region and the distance CD are about $200 h^{-1}$ Mpc and $40 h^{-1}$ Mpc, respectively ($H_0 = 100 h^{-1}$ km sec $^{-1}$ Mpc $^{-1}$), and when the gaps of density and Hubble parameters are ≈ 0.5 and 18%, respectively.

Subject headings: cosmic microwave background - cosmology: large scale structure of the universe - observations

1. Introduction

The dipole moment in the cosmic background radiation (CMB) is thought to come mainly from the Doppler shift due to the motion of the Local Group (LG), relative to the cosmic homogeneous expansion. As the main gravitational source which brings the velocity vector of LG, the existence of the Great Attractor (GA) was found by Lynden-Bell et al. (1988) and Dressler (1987). It has the position at the redshift of 4300 km sec $^{-1}$. On the other hand, the motion of LG in the inertial frame consisting of many clusters on larger-scales was studied observationally by several groups: A bulk flow of ~ 700 km sec $^{-1}$ was found by Lauer and Postman (1994) and Colless (1995) as the motion of the Abell cluster inertial frame relative to LG in the region with redshift < 15000 km

sec^{−1}, but in the other approach the different result was derived by Giovanelli et al. (1998), Dale et al. (1999) and Riess et al. (1997) in the regions with similar redshifts. The Lauer and Postman’s work is based on the assumption that the brightest cluster galaxies as standard candles and the Hoessel relation can be used, but at present these assumptions have been regarded as questionable or unreliable.

Independently of these works, the motion of cluster frames relative to CMB was measured by Hudson et al. (1999) and Willick (1999) due to the global Hubble formula using the Tully-Fisher distances of clusters and their redshifts with respect to CMB, and the flow velocity vector was derived in the region with about $150h^{-1}$ Mpc ($H_0 = 100h^{-1}$ km sec^{−1} Mpc^{−1}). The remarkable and puzzling properties of these flows are that the flow velocity reaches a large value ~ 700 km/sec on large scale, while the dipole velocity (not due to GA) determined in the form of CMB dipole anisotropy seems to be much small, compared with the above flow velocity.

If the observed large-scale matter motion is caused by the attraction from an over-density region containing superclusters, the corresponding velocity must be so large as the large-scale flow velocity and it must be reflected in the form of CMB dipole anisotropy. If this motion is caused in the spherical void-like region, however, the situation is different, because CMB dipole anisotropy near the center can be relatively small in spite of the large-scale flow, as was shown in our previous paper (Tomita 1996). In this previous paper an inhomogeneous model on super-horizon scale was considered to explain the number evolution of QSOs (Tomita 1995), but the relative smallness of the dipole anisotropy can be found independently of the scale of inhomogeneities. The local void region was studied independently by Zehavi et al. (1998) as the local Hubble bubble, which has the scale $\sim 70h^{-1}$ Mpc and is bordered by the dense walls. They analyzed the statistical relation between the distances and the local Hubble constants derived from the data of SNIa, and found the existence of a void region with a local Hubble constant larger than the global Hubble constant. The relation to the SNIa data on larger scales will be discussed from our standpoint in a subsequent paper.

In the present paper we consider more realistic inhomogeneous models on sub-horizon scale, corresponding to matter flows $\sim 150h^{-1}$ Mpc, which may be associated with large-scale structures or excess powers observed by Broadhurst et al. (1990), Landy et al. (1996), and Einasto et al. (1997). In §2, we treat a spherically symmetric inhomogeneous model which consists of inner and outer homogeneous regions connected by a shell being a singular layer, and study the behavior of large-scale motions caused in the inner region, where the present inner density parameter is smaller than the present outer density parameter and the present Hubble parameter in the inner region is larger than that in the outer region (a bulk motion in the void-like region was discussed also by Nakao et al. (1995)). In this section we treat the single-shell case. The double-shell case and a model with an intermediate self-similar region are treated in Appendixes A and B, respectively. In §3, we consider light rays which are emitted at the last scattering surface and reach an observer situated at a point O deviated from the center C, and CMB dipole and quadrupole anisotropies are analyzed. The peculiar velocity of the above large-scale motions and the velocity corresponding

to the CMB dipole anisotropy are compared. In §4, a naive explanation about why CMB dipole anisotropy is small around the center C is shown. In §5 the consistency of the present models with several recent observations of bulk flows is discussed, and in §6 concluding remarks are presented.

2. Inhomogeneous models and the bulk motion

In this section we consider spherically symmetric inhomogeneous cosmological models which have two homogeneous regions connected with a spherical shell, as shown in Fig. 1.

The line-elements in the inner region V^I and the outer region V^{II} are described as

$$ds^2 = g_{\mu\nu}^j(dx^j)^\mu(dx^j)^\nu = -c^2(dt^j)^2 + [a^j(t^j)]^2 \left\{ d(\chi^j)^2 + [f^j(\chi^j)]^2 d\Omega^2 \right\}, \quad (1)$$

where j (= I or II) represents the regions, $f^j(\chi^j) = \sin \chi^j, \chi^j$ and $\sinh \chi^j$ for $k^j = 1, 0, -1$, respectively, and $d\Omega^2 = d\theta^2 + \sin^2 \theta d\varphi^2$. The shell is a time-like hypersurface Σ given as $\chi^I = \chi_1^I$ and $\chi^{II} = \chi_1^{II}$.

2.1. Cosmological models

The Einstein equations are divided into the equations in the two regions and the jump conditions at the shell. The general formulation of the jump condition at the singular surface was derived by Israel (1966) and the concrete expressions of conditions were derived by Maeda (1986) and Sakai et al. (1993). Here the expressions by Sakai et al. are shown using the circumferential radius of the shell R , the velocity of the shell v^j , the Lorentz factor γ^j and the Hubble expansion parameter H^j in V^j ($j = I$ and II) defined by

$$R \equiv a^I f^I = a^{II} f^{II}, \quad v^j \equiv a_j \frac{d\chi^j}{dt^j}, \quad \gamma^j \equiv 1/\sqrt{1 - \left(\frac{v^j}{c}\right)^2} \quad \text{and} \quad H^j \equiv \frac{da^j/dt^j}{a^j}. \quad (2)$$

The Einstein equations for the pressureless matter in the two regions are

$$(H^j)^2 + k^j c^2/(a^j)^2 = \frac{8\pi G}{3} \rho^j + \frac{1}{3} \Lambda c^2, \quad (3)$$

where ρ^j is the mass density of matter ($\propto 1/(a^j)^3$).

The equations for the surface density σ and the velocity v^{II} of the shell are expressed as

$$\gamma^{II} d(4\pi R^2 \sigma)/dt^{II} = \left[4\pi R^2 \gamma^2 v \rho \right]^{II,I}, \quad (4)$$

$$d(\gamma^{II} v^{II})/dt^{II} = -\gamma^{II} v^{II} H^{II} + 2\pi G \sigma - [\gamma^2 v^2 \rho]^{II}/\sigma, \quad (5)$$

where $[\Phi]^{II,I} \equiv \Phi^{II} - \Phi^I$. The conditions of continuity of the metric ($d\tau^2 = -ds^2$) and the common velocity $dR/d\tau$ reduce to

$$dt^I/dt^{II} = \gamma^I/\gamma^{II} \quad (6)$$

and

$$\gamma^I(f'^I v^I + H^I R) = \gamma^{II}(f'^{II} v^{II} + H^{II} R), \quad (7)$$

where $f'^j = df^j(\chi^j)/d\chi^j$.

Another important component of jump conditions playing a role of a constraint equation is

$$[\gamma(f' + vHR)]^{II,I} = -4\pi G\sigma R. \quad (8)$$

Solving Eqs.(4) and (5) we can obtain the time evolution of σ and v_{II} in the shell, and v^I is derived using Eq.(7). These values of σ , v^I and v^{II} satisfy the condition (8). The initial condition is given as a form of $(H^I)_i = (H^{II})_i$ at an initial epoch $(t^j)_i$ such as the recombination epoch.

The background models in V^I and V^{II} are rewritten using

$$y^j \equiv a^j/(a_0)^j, \quad \tau^j \equiv H_0^j t^j, \quad \lambda_0^j \equiv \frac{1}{3}\Lambda c^2/(H_0^j)^2, \quad \Omega_0^j \equiv \frac{8\pi G}{3(H_0^j)^2}(\rho_0)^j, \quad (9)$$

where 0 denotes the present epoch. Eq. (3) is given as

$$dy^j/d\tau^j = (y^j)^{-1/2} P_j(y^j), \quad (10)$$

where

$$P_j(y^j) \equiv [\Omega_0^j + \lambda_0^j(y^j)^3 + (1 - \Omega_0^j - \lambda_0^j)y^j]^{1/2} \quad (11)$$

and $(a_0)^j$ is given by

$$(a_0 H_0)^j = 1/\sqrt{1 - \Omega_0^j - \lambda_0^j}. \quad (12)$$

The conformal times η^j are defined by

$$\eta^j \equiv \sqrt{1 - \Omega_0^j - \lambda_0^j} \int_0^{y^j} dy/[y^{1/2} P_j(y)]. \quad (13)$$

The solution of Eq. (10) in the case of $k^I = k^{II} = -1$ and $\Lambda = 0$ are expressed as

$$y^j = \frac{\Omega_0^j}{2(1 - \Omega_0^j)}(\cosh \eta^j - 1), \quad (14)$$

$$\tau^j = \frac{\Omega_0^j}{2(1 - \Omega_0^j)^{3/2}}(\sinh \eta^j - \eta^j). \quad (15)$$

In the case of nonzero Λ , Eq. (10) is solved numerically.

Eqs. (4) and (5) were solved by Sakai et al. (1993) and it was shown in the case of $\Omega_i \simeq 1$ that the present value of v^{II} at $a/a_i > 100$ is < 100 km/s, as long as the shell starts with the vanishing initial velocity $(v^j)_i = 0$.

Here the initial condition $(H^I)_i = (H^{II})_i$ at initial epoch $y^j = (y^j)_i$ is expressed as

$$\begin{aligned} H_0^I &= (y_i^I)^{-3/2} [\Omega_0^I + \lambda_0^I (y_i^I)^3 + (1 - \Omega_0^I - \lambda_0^I) y_i^I]^{1/2} \\ &= H_0^{II} (y_i^{II})^{-3/2} [\Omega_0^{II} + \lambda_0^{II} (y_i^{II})^3 + (1 - \Omega_0^{II} - \lambda_0^{II}) y_i^{II}]^{1/2}, \end{aligned} \quad (16)$$

where we have

$$\frac{\Omega_0^{II}}{\Omega_0^I} = \frac{\rho_0^{II}}{\rho_0^I} \left(\frac{H_0^I}{H_0^{II}} \right)^2, \quad \frac{\lambda_0^{II}}{\lambda_0^I} = \left(\frac{H_0^I}{H_0^{II}} \right)^2 \quad (17)$$

from Eq. (9). If we eliminate $\Omega_0^{II}, \lambda_0^{II}$ from Eq. (16) using Eq. (17), we obtain

$$\left[\frac{\rho_0^{II}}{\rho_0^I} (1 - y_i^{II}) - \left(\frac{y_i^{II}}{y_i^I} \right)^3 (1 - y_i^I) \right] \Omega_0^I - \left[1 - \left(\frac{y_i^{II}}{y_i^I} \right)^2 \right] y_i^{II} \lambda_0^I + \left[\left(\frac{H_0^{II}}{H_0^I} \right)^2 - \left(\frac{y_i^{II}}{y_i^I} \right)^3 \right] y_i^{II} = 0. \quad (18)$$

Since $y_i^I \sim y_i^{II} \sim 10^{-3}$ ($\ll 1$), we assume

$$\frac{\rho_0^{II}}{\rho_0^I} = \left(\frac{y_i^{II}}{y_i^I} \right)^3 (1 + \epsilon y_i^I), \quad (19)$$

where $\epsilon \approx 1$. Then we get from Eq. (18)

$$\left(\frac{H_0^{II}}{H_0^I} \right)^2 = \left(\frac{y_i^{II}}{y_i^I} \right)^3 + \left[1 - \left(\frac{y_i^{II}}{y_i^I} \right)^2 \right] \lambda_0^I + \left(\frac{y_i^{II}}{y_i^I} \right)^3 \left[1 - (1 + \epsilon) \frac{y_i^I}{y_i^{II}} \right] \Omega_0^I. \quad (20)$$

If we give $\Omega_0^I, \lambda_0^I, \epsilon$ and y_i^{II}/y_i^I , therefore, we can obtain H_0^{II}/H_0^I for Eq. (20) and derive ρ_0^{II}/ρ_0^I from Eq. (20) and Ω_0^{II}/Ω_0^I and $\lambda_0^{II}/\lambda_0^I$ from Eq. (17). From Eqs. (17), (19) and (20), we find that $H_0^{II}/H_0^I < 1$ and $\Omega_0^{II}/\Omega_0^I > 1$, if

$$1 > \frac{y_i^{II}}{y_i^I} > 1 + \left[1 - \left(\frac{y_i^{II}}{y_i^I} \right)^2 \right] \left(\frac{y_i^I}{y_i^{II}} \right)^3 \lambda_0^I + \left[1 - (1 + \epsilon) \frac{y_i^I}{y_i^{II}} \right] \Omega_0^I. \quad (21)$$

In the case $\Lambda = 0$, we have an example for $\Omega_0^I = 0.2$

$$\Omega_0^{II} = 0.56, \quad H_0^{II}/H_0^I = 0.80, \quad \rho_0^{II}/\rho_0^I = 1.8, \quad y_i^{II}/y_i^I = 1.2, \quad \epsilon = 4.1. \quad (22)$$

In the case $\Lambda \neq 0$, we have an example

$$\lambda_0^I = 0.672, \quad \lambda_0^{II} = 0.43, \quad \Omega_0^I = 0.3, \quad \Omega_0^{II} = 0.563, \quad H_0^{II}/H_0^I = 0.80, \quad \epsilon = 0.64, \quad (23)$$

so that

$$\Omega_0^I + \lambda_0^I = 0.872, \quad \Omega_0^{II} + \lambda_0^{II} = 0.993. \quad (24)$$

2.2. Bulk motion

Now let us consider the velocity field around an observer O in V^I at the point with $l_0 \equiv (a\chi)_0 \ll (a\chi)_1$. Since l_0 is much smaller than the curvature radius, we can approximately neglect the spatial curvature around him. Then he has the relative velocity

$$\Delta v_0 = (H_0^I - H_0^{II})l_0 \quad (25)$$

to matter in the outer region in the direction of the X axis. If $H_0^I = 100h$ km/sec/Mpc, $H_0^{II} = 0.82H_0^I$ and $l_0 = 40h^{-1}$ Mpc, we have $\Delta v_0 = 720$ km/sec.

Here consider a galaxy G with the radius coordinate χ and angle φ . Then the relative velocity of G to matter in the outer region is

$$\Delta v_G = (H_0^I - H_0^{II})(a_0\chi) \quad (26)$$

in the radial direction from the center C of the inner region (cf. Fig. 3).

This velocity can be divided into the X component $(\Delta v_G)_X$ and the line-of-sight component $(\Delta v_G)_{LS}$ with respect to the observer O as follows, noticing that the angle $\angle GOX$ ($= \phi$) satisfies the relation

$$\sin \phi = \chi \sin \varphi / [\chi^2 + \chi_0^2 - 2\chi\chi_0 \cos \varphi]^{1/2}, \quad \cot \phi = (\cos \varphi - \chi_0/\chi) / \sin \varphi. \quad (27)$$

Their values are

$$(\Delta v_G)_X = \Delta v_G \sin(\phi - \varphi) / \sin \phi = \Delta v_0, \quad (28)$$

$$(\Delta v_G)_{LS} = \Delta v_G \sin \varphi / \sin \phi = \Delta v_G [1 - 2(\chi_0/\chi) \cos \varphi + (\chi_0/\chi)^2]^{1/2} \simeq \Delta v_G. \quad (29)$$

That is, the X component $(\Delta v_G)_X$ is constant and equal to Δv_0 , and another component, which is in the line-of-sight direction from the observer, is nearly equal to Δv_G . Because the first component $(\Delta v_G)_X$ is independent of the position, it can be interpreted as the peculiar velocity v_p of galaxies which represents the bulk motion:

$$v_p = (\Delta v_G)_X = \Delta v_0. \quad (30)$$

3. Redshift formula and the CMB anisotropy

The wavevector k^μ in the inner and outer regions in the plane of $\theta = \pi/2$ is obtained by solving null-geodesic equation and expressed as

$$(k^0)^j = dt^j/d\lambda = \frac{a_0^j}{a^j} w_1^j, \quad (31)$$

$$(k^\chi)^j = d\chi^j/d\lambda = \pm \frac{a_0^j w_1^j}{(a^j)^2} \left[1 - \left(\frac{d^j/w_1^j}{a_0^j \sinh \chi^j} \right)^2 \right]^{1/2}, \quad (32)$$

$$(k^\varphi)^j = d\varphi/d\lambda = d^j / \left(a^j \sinh \chi^j \right)^2, \quad (33)$$

where $j = I$ and II , and λ is an affine parameter.

3.1. Light paths

In the inner region V^I , it is assumed that at the present epoch ($t^I = t_0^I$) all rays reach an observer at the point O with $\chi = \chi_0$, $\theta = \pi/2$ and $\varphi = 0$ in the X axis, and the angle between the rays and the X axis is ϕ . Then we have

$$\phi = \phi_1 \quad \text{and} \quad \pi - \phi_1, \quad (34)$$

where

$$\phi_1 \equiv \sin^{-1} \left[\frac{d^I/w_1^I}{a_0^I \sinh \chi_0^I} \right] (< \pi/2). \quad (35)$$

For $\phi = \phi_1$ the rays are expressed as

$$G(\chi^I) \equiv \cosh^{-1} \left(\frac{\cosh \chi^I}{h_0^I} \right) - \cosh^{-1} \left(\frac{\cosh \chi_0^I}{h_0^I} \right) = \eta_0^I - \eta^I, \quad (36)$$

where

$$h_0^j \equiv \left[1 + \left(\frac{d^j/w_1^j}{(a_0)^j} \right)^2 \right]^{1/2}, \quad (37)$$

η^I is defined by Eqs. (13) and (14), and η_0^I is equal to η^I at present epoch ($y^I = 1$).

For $\phi = \pi - \phi_1$ we have

$$\begin{aligned} G(\chi^I) &= -\eta_0^I + \eta^I, & \text{for } \eta_0^I \geq \eta^I > \eta_m, \\ &= -\eta^I - \eta_0^I + 2\eta_m, & \text{for } \eta^I \leq \eta_m, \end{aligned} \quad (38)$$

where

$$\eta_m \equiv \eta_0^I - \cosh^{-1} \left(\frac{\cosh \chi_0^I}{h_0^I} \right). \quad (39)$$

In the latter case, χ^I has the minimum value (i.e., $k^\chi = 0$) at $\eta^I = \eta_m$.

At the boundary $\eta^I = \eta_1^I$ and $\chi^I = \chi_1^I$, therefore, we obtain

$$\eta_1^I = \eta_0^I \pm \cosh^{-1} \left(\frac{\cosh \chi_0^I}{h_0^I} \right) - \cosh^{-1} \left(\frac{\cosh \chi_1^I}{h_0^I} \right) \quad (40)$$

for $\phi = \begin{pmatrix} \phi_1 \\ \pi - \phi_1 \end{pmatrix}$, respectively. In the outer region V^{II} , we have

$$G(\chi^{II}) \equiv \cosh^{-1} \left(\frac{\cosh \chi^{II}}{h_0^{II}} \right) - \cosh^{-1} \left(\frac{\cosh \chi_1^{II}}{h_0^{II}} \right) = \eta_1^{II} - \eta^{II}, \quad (41)$$

where η^{II} is given by Eqs. (13) and (14), and η_1^{II} and χ_1^{II} are the values at the shell. At the recombination epoch we have

$$\eta_{\text{rec}}^{II} = \eta_1^{II} - \cosh^{-1} \left(\frac{\cosh \chi_{\text{rec}}^{II}}{h_0^{II}} \right) + \cosh^{-1} \left(\frac{\cosh \chi_1^{II}}{h_0^{II}} \right). \quad (42)$$

The junction of wavevectors at the boundary is expressed as

$$(k^0)^I = (k^0)^{II}, \quad (43)$$

$$(\sqrt{g_{\chi\chi}} k^\chi)^I = (\sqrt{g_{\chi\chi}} k^\chi)^{II}, \quad (44)$$

$$(\sqrt{g_{\varphi\varphi}} k^\varphi)^I = (\sqrt{g_{\varphi\varphi}} k^\varphi)^{II}. \quad (45)$$

Eqs. (43) and (45) give

$$\left(\frac{a_0}{a_1}\right)^I w_1^I = \left(\frac{a_0}{a_1}\right)^{II} w_1^{II}, \quad (46)$$

$$d^I = d^{II}, \quad (47)$$

respectively, where we used the relation $R = (af)^I = (af)^{II}$. The conditions (43) and (45) are evidently consistent with Eq. (44), since k^μ is a null vector.

3.2. Redshift formula

Now let us derive the redshift formula for rays which are emitted at the recombination epoch. Here this epoch is defined as the time of the radiation temperature $T_r = 10^3 (T_r)_0$ in the region V^{II} , where $(T_r)_0$ is the present temperature ($\simeq 2.7$ K). The total redshift factor $(1 + z_{\text{rec}})$ is calculated as the product of two redshift factors which are caused in the two regions V^I and V^{II} .

First we assume that the shell is comoving and later the correction due to the motion of the shell is examined. If we consider a virtual observer at the center C ($\chi = 0$), a light ray which is received by him at $\bar{\eta}^I = \bar{\eta}_0^I$ is expressed as

$$\bar{\eta}_0^I - \bar{\eta}^I = \chi^I, \quad \bar{\eta}_0^I - \bar{\eta}_1^I = \chi_1^I \quad (48)$$

in V^I , and

$$\bar{\eta}_{\text{rec}}^{II} - \bar{\eta}^{II} = \chi_{\text{rec}}^{II} - \chi^{II}, \quad \bar{\eta}_{\text{rec}}^{II} - \bar{\eta}_1^{II} = \chi_{\text{rec}}^{II} - \chi_1^{II} \quad (49)$$

in V^{II} , when the ray is emitted at the recombination epoch.

The redshift factors are

$$1 + \bar{z}_1^I = \frac{a_0^I}{a^I(\bar{\eta}_1^I)} = \frac{1}{y^I(\bar{\eta}_1^I)} \quad (50)$$

in V^I , and

$$\frac{1 + \bar{z}_{\text{rec}}^{II}}{1 + \bar{z}_1^{II}} = \frac{a^{II}(\bar{\eta}_1^{II})}{a^{II}(\bar{\eta}_{\text{rec}}^{II})} = \frac{y^{II}(\bar{\eta}_1^{II})}{y^{II}(\bar{\eta}_{\text{rec}}^{II})} \quad (51)$$

in V^{II} . The junction condition in Eq. (6) gives $\bar{z}_1^I = \bar{z}_1^{II}$ for $v^I = v^{II} = 0$, so that

$$1 + \bar{z}_{\text{rec}}^{II} = \frac{y^{II}(\bar{\eta}_1^{II})}{y^{II}(\bar{\eta}_{\text{rec}}^{II})y^I(\bar{\eta}_1^I)}. \quad (52)$$

Here we specify the value of \bar{z}_1^I as $\bar{z}_1^I = 0.067 \sim 0.1$. Then $\bar{\eta}_1^I$ and χ_1^I are determined from Eqs. (48) and (50), and $\bar{\eta}_1^{II}$ and χ_1^{II} are determined using the relations

$$a_0^I y^I(\bar{\eta}_1^I) \sinh \chi_1^I = a_0^{II} y^{II}(\bar{\eta}_1^{II}) \sinh \chi_1^{II} \quad (53)$$

and

$$a_0^I \int_0^{\bar{\eta}_1^I} y^I(\eta^I) d\eta^I = a_0^{II} \int_0^{\bar{\eta}_1^{II}} y^{II}(\eta^{II}) d\eta^{II}, \quad (54)$$

which are obtained from Eqs. (2) and (6). If $\bar{z}_{\text{rec}}^{II}$ is moreover specified (in the following we take the value $\bar{z}_{\text{rec}}^{II} = 10^3 - 1$), $y(\bar{\eta}_{\text{rec}})$ or $\bar{\eta}_{\text{rec}}$ is determined using Eq. (52).

Next we consider the observer at O (with $\chi^I = \chi_0^I$ and $\varphi = 0$). The above determined χ_1^j ($j = I$ and II) and η_{rec}^j ($= \bar{\eta}_{\text{rec}}^{II}$) are used also for rays reaching this observer, to identify the position of the shell and the recombination epoch. It should be noted that η_{rec}^j depends only on the temperature at the recombination epoch and is independent of the existence of the inner region V^I .

In V^I we have the redshift

$$1 + z_1^I = \frac{a_0^I}{a^I(\eta_1^I)} = \frac{1}{y^I(\eta_1^I)} \quad (55)$$

and in V^{II} we have

$$\frac{1 + z_{\text{rec}}^{II}}{1 + z_1^{II}} = \frac{a^{II}(\eta_1^{II})}{a^{II}(\eta_{\text{rec}}^{II})} = \frac{y^{II}(\eta_1^{II})}{y^{II}(\eta_{\text{rec}}^{II})}. \quad (56)$$

For a given χ_1^I , we obtain η_1^I by solving Eq. (40) and obtain z_1^I from Eq. (55). The junction condition in Eq. (6) gives $z_1^I = z_1^{II}$, and η_1^{II} is related to η_1^I using the relations (53) and (54). Then the product of Eqs. (55) and (56) reduces to

$$1 + z_{\text{rec}}^{II} = \frac{y^{II}(\eta_1^{II})}{y^I(\eta_1^I) y^{II}(\eta_{\text{rec}}^{II})}, \quad (57)$$

which is given as a function of angle ϕ .

Now let us consider the case when the shell is not comoving, i.e., $v^I \neq 0$, $v^{II} \neq 0$. As was shown by Sakai et al., the velocities are < 200 km/sec and $(v^j/c)^2 < 10^{-7}$ for $j = I$ and II . Accordingly, we can assume $\gamma^j = 1$ for $j = I$ and II , so that the condition $z_1^I = z_1^{II}$ and Eq. (54) hold. In order to take the shell motion into account, we assume the relation

$$\chi_1^I = (\chi_1^I)_{\phi=0} + v^I [\eta_1^I - (\eta_1^I)_{\phi=0}] \quad (58)$$

in Eq. (40) for arbitrary ϕ , where $(\chi_1^I)_{\phi=0}$ and $(\eta_1^I)_{\phi=0}$ are their values for the ray incident in the direction of $\phi = 0$. Subsequent calculations are same as the calculations for $v^I = 0$.

The derivations of z_{rec}^{II} in the case of double shells and in the inhomogeneous model with an intermediate self-similar region are shown in Appendixes A and B.

3.3. CMB anisotropy

The values of $z_{\text{rec}}^{\text{II}}$ are numerically calculated for $0 < \phi < \pi$, and their dipole and quadrupole moments are derived. When z_{rec} ($= z_{\text{rec}}^{\text{II}}(\phi)$) is given, the temperature $T(\phi)$ of the cosmic background radiation is proportional to $1/(1+z_{\text{rec}})$, and the dipole moment D and quadrupole moment Q are defined as

$$D \equiv \left| \int_0^\pi \int_0^{2\pi} (1+z_{\text{rec}})^{-1} Y_{10} \sin \phi d\phi d\varphi \right| / \langle (1+z_{\text{rec}})^{-1} \rangle, \quad (59)$$

$$Q \equiv \left| \int_0^\pi \int_0^{2\pi} (1+z_{\text{rec}})^{-1} Y_{20} \sin \phi d\phi d\varphi \right| / \langle (1+z_{\text{rec}})^{-1} \rangle, \quad (60)$$

where $\langle \rangle$ means the average value taken over the whole sky, and

$$Y_{10}(\phi) = \sqrt{\frac{3}{4\pi}} \cos \phi \quad Y_{20}(\phi) = \sqrt{\frac{5}{4\pi}} \left(\frac{3}{2} \cos^2 \phi - \frac{1}{2} \right). \quad (61)$$

The Doppler velocity v_d corresponding to D is given by

$$v_d \equiv c[(3/4\pi)^{1/2} D]. \quad (62)$$

Assuming l_0 ($\equiv a_0 \chi_0$) $= 40(h^{\text{I}})^{-1}$ Mpc mainly, D, Q and v_d were derived for various model parameters. Their values in models with a single shell and double shells are shown in Tables 1 and 2, respectively. The values in models with an intermediate self-similar region are shown in Table 3. In Table 1 the values in the case with a moving shell are shown.

It is found from Table 1 that (1) v_d/v_p is smaller than 0.17 in all cases, (2) v_d is approximately proportional to l_0 (as well as v_p), (3) v_d is smaller for smaller $(\Omega_0^{\text{II}} - \Omega_0^{\text{I}})$ and $(h^{\text{I}} - h^{\text{II}})$, (4) the positive cosmological constant plays a role of increasing v_d , and (5) the influence of the shell motion on D, Q and v_d is negligibly small.

If we compare two lines in Table 2 with the corresponding ones (the first line and 8th line) in Table 1, the results in the models with a single shell and double shells are found to be quite consistent. Moreover, if we compare four lines in Table 3 with the corresponding ones (the second line, 4th and 6th line) in Table 1, the results in the models with a single shell and a self-similar region are found to be similarly consistent. Accordingly v_d/v_p is ≈ 0.1 in all models we treated here.

4. Naive derivation of redshift factors

For the dipole anisotropy the maximum difference of temperatures and redshifts can be seen in a direction ($\phi = \phi_1$) and the inverse direction ($\phi = \pi - \phi_1$). Here let us compare the redshifts in the directions $\phi = 0$ and π appearing in the model with a single shell. The spatial curvature

is neglected for simplicity. In the X axis we consider six points O, A, B, C, D, and E, for which $X = \chi_0, \chi_1, \chi_1 + 2\chi_0, 0, -\chi_1$, and $-\chi_1 + 2\chi_0$, as shown in Fig. 4.

Points B and D have the equal distance from the observer's point O.

The redshifts $z_{\text{rec}}(0)$ and $z_{\text{rec}}(\pi)$ of the rays from another points P and P' at the recombination epoch to the observer at O in the directions $\phi = 0$ and π are divided into three steps

$(P \rightarrow B, B \rightarrow A, A \rightarrow O)$ and $(P' \rightarrow D, D \rightarrow E, E \rightarrow O)$,

respectively. That is,

$$1 + z_{\text{rec}}(0) = (1 + z_{PB})(1 + z_{BA})(1 + z_{AO}), \quad 1 + z_{\text{rec}}(\pi) = (1 + z_{P'D})(1 + z_{DE})(1 + z_{EO}). \quad (63)$$

Among these three steps, the first and third steps have equal redshifts evidently : $z_{PB} = z_{P'D}$, $z_{AO} = z_{EO}$. In the processes $(B \rightarrow A)$ and $(D \rightarrow E)$, we have the redshifts due to the cosmic expansion, the Doppler shift and the gravitational redshift. The expansion redshift factors in V^{II} and V^{I} are

$$[1 + H_0^{\text{II}}(2a_0\chi_0/c)], \quad [1 + H_0^{\text{I}}(2a_0\chi_0/c)], \quad (64)$$

respectively. The Doppler shifts at A and D due to the relative velocity between V^{I} and V^{II} frames are

$$[1 - \frac{1}{c}(H_0^{\text{I}} - H_0^{\text{II}})a_0(\chi_1 - \chi_0)], \quad [1 - \frac{1}{c}(H_0^{\text{I}} - H_0^{\text{II}})a_0(\chi_1 + \chi_0)], \quad (65)$$

respectively. The gravitational redshifts are represented by potentials ψ_{BA} and ψ_{DE} given by

$$\psi_{BA} \equiv \frac{4\pi G(a_0)^3}{c^2} \left[\frac{1}{3} \frac{\rho_0^{\text{I}}(\chi_1)^3}{\chi_1 + \chi_0} + \frac{\rho_0^{\text{II}}(\chi_1 + \chi_0)^2 \chi_0}{\chi_1 + \chi_0} \right], \quad (66)$$

$$\psi_{DE} \equiv \frac{4\pi G(a_0)^3}{c^2} \left[\frac{1}{3} \frac{\rho_0^{\text{I}}(\chi_1)^3}{\chi_1 + \chi_0} - \frac{\rho_0^{\text{II}}(\chi_1 - \chi_0)^2 \chi_0}{\chi_1 - \chi_0} \right]. \quad (67)$$

Accordingly the total redshift factors are

$$\begin{aligned} 1 + z_{BA} &= [1 + H_0^{\text{II}}(2a_0\chi_0/c)][1 - \frac{1}{c}(H_0^{\text{I}} - H_0^{\text{II}})a_0(\chi_1 - \chi_0)][1 + \psi_{BA}] \\ &= 1 - \frac{a_0}{c}(H_0^{\text{I}} - H_0^{\text{II}})\chi_1 + \frac{a_0}{c}(H_0^{\text{I}} + H_0^{\text{II}})\chi_0 + \psi_{BA} \\ &\quad - \left(\frac{a_0}{c}\right)^2 H_0^{\text{II}}(H_0^{\text{I}} - H_0^{\text{II}})\chi_0(\chi_1 - \chi_0) + \dots, \end{aligned} \quad (68)$$

$$\begin{aligned} 1 + z_{DE} &= [1 + H_0^{\text{I}}(2a_0\chi_0/c)][1 - \frac{1}{c}(H_0^{\text{I}} - H_0^{\text{II}})a_0(\chi_1 + \chi_0)][1 + \psi_{DE}] \\ &= 1 - \frac{a_0}{c}(H_0^{\text{I}} - H_0^{\text{II}})\chi_1 + \frac{a_0}{c}(H_0^{\text{I}} + H_0^{\text{II}})\chi_0 + \psi_{DE} \\ &\quad - \left(\frac{a_0}{c}\right)^2 H_0^{\text{I}}(H_0^{\text{I}} - H_0^{\text{II}})\chi_0(\chi_1 + \chi_0) + \dots. \end{aligned} \quad (69)$$

The difference of these factors reduces to

$$z_{\text{rec}}(0) - z_{\text{rec}}(\pi) \simeq z_{BA} - z_{DE}$$

$$\simeq \psi_{\text{BA}} - \psi_{\text{DE}} + \left(\frac{a_0}{c}\right)^2 (H_0^{\text{I}} - H_0^{\text{II}}) \chi_0 \left[(H_0^{\text{I}} + H_0^{\text{II}}) \chi_0 + (H_0^{\text{I}} - H_0^{\text{II}}) \chi_1 \right]. \quad (70)$$

That is, the main terms in $(1 + z_{\text{BA}})$ and $(1 + z_{\text{DE}})$ cancel. The ratio \mathcal{R} of $[z_{\text{rec}}(0) - z_{\text{rec}}(\pi)]$ to the relative velocity between V^{I} and V^{II} is

$$\begin{aligned} \mathcal{R} \equiv \frac{z_{\text{rec}}(0) - z_{\text{rec}}(\pi)}{(H_0^{\text{I}} - H_0^{\text{II}}) a_0 \chi_0 / c} &\simeq \frac{3}{4} \left[\Omega_0^{\text{II}} (H_0^{\text{II}})^2 (\chi_1 + \chi_0) - \Omega_0^{\text{I}} (H_0^{\text{I}})^2 (\chi_1 - \chi_0) \right] / (H_0^{\text{I}} - H_0^{\text{II}}) \\ &\quad + 2(H_0^{\text{I}} + H_0^{\text{II}}) \chi_0 / c + 2(H_0^{\text{I}} - H_0^{\text{II}}) \chi_1 / c, \end{aligned} \quad (71)$$

where we used Eq.(9) for ρ_0^j . This ratio is the counterpart of the ratio of the velocity v_d (corresponding to the dipole moment) to the relative (peculiar) velocity v_p , and these two ratios have comparable values.

5. Consistency with the observed large-scale bulk flows

As was shown in B of §2, the bulk velocities in all positions within the region I are equal in the present models, so that the relative velocity (v_{LG}) of LG to the cluster frame is only the peculiar velocity of LG caused by GA and the nearby superclusters. Moreover, as was shown in C of §3 the dipole velocity v_d corresponding to the bulk velocity v_p is $\sim 0.1v_p$, and so the total dipole velocity v_{td} of LG to CMB is $v_{td} = v_{\text{LG}} + v_d$ ($\sim 0.1v_p$) $\cong v_{\text{LG}}$.

These conclusions are consistent as follows with (1) the observed velocities (v_{LG}) of LG with respect to the cluster frames by Giovanelli et al. (1998), Dale et al. (1999) and Riess et al. (1997), which are nearly equal to the total dipole velocity (v_{td}) with respect to CMB, and (2) the bulk velocities (v_p) in the SMAC observation (Hudson et al. (1999)) and the LP10k observation (Willick (1999)) are ~ 700 km sec $^{-1}$ in the nearly same directions:

According to Dale et al. (1999), we have $v_{\text{LG}} = 565 \pm 113$ km sec $^{-1}$ and $(l, b) = (267^\circ, 26^\circ) \pm 10^\circ$. On the other hand, $v_{td} = 627 \pm 22$ km sec $^{-1}$ and $(l, b) = (276^\circ, 30^\circ)$ (Kogut et al. (1993)). Since both directions are nearly equal, the velocity difference is about 60 km sec $^{-1}$. This value is comparable with v_d ($\sim 0.1v_p$), in the consistent manner with the result in the present models.

However, they are inconsistent with the observations of Lauer and Postman (1994) and Colless (1995) in which v_{td} and v_{LG} are in quite different directions. At present these observations seem to have been ruled out (cf. Proceedings of the International Conference on Cosmic Flows 1999).

6. Concluding remarks

In this paper we considered the behaviors of galaxies and light rays in spherically symmetric inhomogeneous models consisting of inner and outer homogeneous regions V^{I} and V^{II} with Ω_0^{I} and Ω_0^{II} ($> \Omega_0^{\text{I}}$) and H_0^{I} and H_0^{II} ($< H_0^{\text{I}}$), respectively, connected by a single shell. In Appendixes we

treated also the models with double shells and an intermediate self-similar region. It was shown as the result that when we observe the motion of galaxies at the point O deviated from the center C in V^I , a constant peculiar velocity component v_p appears in the direction from the center to the observer ($C \rightarrow O$). Moreover it was shown that the velocity v_d corresponding to the dipole anisotropy of CMB radiation is by a factor ≈ 10 small compared with v_p . This result may fit for the observed situation of the cosmic flow of cluster galaxies, when the scale of the inner region and the distance CO are about $200(h^I)^{-1}$ and $40(h^I)^{-1}$ Mpc, respectively, and when $(\Omega_0^{II} - \Omega_0^I)$ is ≈ 0.5 and $(H_0^I - H_0^{II})$ is $\approx 18h^I$ km/sec/Mpc (or $h^{II}/h^I \approx 0.82$), respectively. This difference of the Hubble parameters may be consistent with their recent values due to nearby and remote observations, because short and long distance scales give the Hubble constant of $H_0 \geq 70$ and $H_0 \sim 55$, respectively (Branch 1998; Freedman 1997; Sandage and Tammann 1997; Blandford and Kundić 1997). A model with multi-shells in the region of $100 \sim 300$ Mpc in which the parameters change stepwise will be better to reproduce the observed distribution of the Hubble constant.

It was shown that the present models are consistent with the current observations of large-scale flows (Giovanelli et al. (1998), Dale et al. (1999), Riess et al. (1997), Hudson et al. (1999) and Willick (1999)), but inconsistent with other observations (Lauer and Postman (1994) and Colless (1995)) which may have been ruled out.

It is interesting and important to study the influences of the above inhomogeneity on the cosmological observations such as the magnitude-redshift relation of SN1a, the number count of galaxies, the time delay for lensed QSOs, and so on. They will be quantitatively analyzed and shown in near future.

In this paper the motion of LG due to GA and superclusters in similar distances was not treated, while spherical matter distributions on such scales were analyzed by Humphreys et al. (1997). But the approximation of spherical symmetry may not be good to their small-scale matter distribution.

A. Models with double shells

The spacetime is divided into three homogeneous regions V^I , V^{II} , and V^{III} , as shown in Fig. 5. The cosmological parameters in V^j are shown as Ω_0^j , λ_0^j and so on, where $j = I, II, III$.

Eqs. (1) - (3) and (9) - (15) hold also in region III as well as in regions I and II. The junction condition at the second boundary between V^{II} and V^{III} have similar expressions to those at the first boundary:

$$R \equiv a^{II} f^{II} = a^{III} f^{III}, \quad (A1)$$

$$\gamma^{III} d(4\pi R^2 \sigma) / dt^{III} = \left[4\pi R^2 \gamma^2 v \rho \right]^{III,II}, \quad (A2)$$

$$d(\gamma^{III} v^{III}) / dt^{III} = -\gamma^{III} v^{III} H^{III} + 2\pi G \sigma - [\gamma^2 v^2 \rho]^{III} / \sigma, \quad (A3)$$

$$dt^{\text{II}}/dt^{\text{III}} = \gamma^{\text{II}}/\gamma^{\text{III}}, \quad (\text{A4})$$

$$\gamma^{\text{II}}(f'^{\text{II}}v^{\text{II}} + H^{\text{II}}R) = \gamma^{\text{III}}(f'^{\text{III}}v^{\text{III}} + H^{\text{III}}R), \quad (\text{A5})$$

and

$$[\gamma(f' + vHR)]^{\text{III},\text{II}} = -4\pi G\sigma R, \quad (\text{A6})$$

where $[\Phi]^{\text{III},\text{II}} \equiv \Phi^{\text{III}} - \Phi^{\text{II}}$.

Similarly to Eqs. (19) and (20), moreover, we have

$$\frac{\rho_0^{\text{III}}}{\rho_0^{\text{II}}} = \left(\frac{y_i^{\text{III}}}{y_i^{\text{II}}}\right)^3 (1 + \epsilon y_i^{\text{II}}), \quad (\text{A7})$$

$$\left(\frac{H_0^{\text{III}}}{H_0^{\text{II}}}\right)^2 = \left(\frac{y_i^{\text{III}}}{y_i^{\text{II}}}\right)^3 + \lambda_0^{\text{II}} \left[1 - \left(\frac{y_i^{\text{III}}}{y_i^{\text{II}}}\right)^2\right] + \frac{y_i^{\text{III}}}{y_i^{\text{II}}} \left[1 - (1 + \epsilon) \frac{y_i^{\text{II}}}{y_i^{\text{III}}}\right] \Omega_0^{\text{II}}, \quad (\text{A8})$$

where $\epsilon \approx 1$.

As for light rays, the equations in V^{I} and V^{II} are same as those in Sec. 3, and equations in V^{III} are common with those in V^{II} . At the second boundary ($\eta = \eta_2$, $\chi = \chi_2$) we have

$$\left(\frac{a_0}{a_2}\right)^{\text{II}} w_2^{\text{II}} = \left(\frac{a_0}{a_1}\right)^{\text{III}} w_2^{\text{III}}, \quad (\text{A9})$$

$$d^{\text{II}} = d^{\text{III}}, \quad (\text{A10})$$

where $a_2 = a(\eta_2)$.

Under the assumption that the shells are comoving (i.e., $v^{\text{I}} = v^{\text{II}} = v^{\text{III}} = 0$), we obtain the following redshift formulas:

$$1 + z_1^{\text{I}} = \frac{1}{y^{\text{I}}}(\eta_1^{\text{I}}) \quad (\text{A11})$$

and in V^{II} we have

$$\frac{1 + z_2^{\text{II}}}{1 + z_1^{\text{II}}} = \frac{y^{\text{II}}(\eta_1^{\text{II}})}{y^{\text{II}}(\eta_2^{\text{II}})}. \quad (\text{A12})$$

$$\frac{1 + z_{\text{rec}}^{\text{III}}}{1 + z_2^{\text{III}}} = \frac{y^{\text{III}}(\eta_2^{\text{III}})}{y^{\text{III}}(\eta_{\text{rec}}^{\text{III}})}. \quad (\text{A13})$$

From Eqs. (6) and (A4) we have two equations $z_1^{\text{I}} = z_1^{\text{II}}$ and $z_2^{\text{II}} = z_2^{\text{III}}$. Moreover, $(\eta_1^{\text{II}}, \chi_1^{\text{II}})$ are related to $(\eta_1^{\text{I}}, \chi_1^{\text{I}})$ using Eqs. (53) and (54), and $(\eta_2^{\text{III}}, \chi_2^{\text{III}})$ are related to $(\eta_2^{\text{II}}, \chi_2^{\text{II}})$ using the similar equations

$$a_0^{\text{II}} y^{\text{II}}(\eta_2^{\text{II}}) \sinh \chi_2^{\text{II}} = a_0^{\text{III}} y^{\text{III}}(\eta_2^{\text{III}}) \sinh \chi_2^{\text{III}} \quad (\text{A14})$$

and

$$a_0^{\text{II}} \int_0^{\eta_2^{\text{II}}} y^{\text{II}}(\eta^{\text{II}}) d\eta^{\text{II}} = a_0^{\text{III}} \int_0^{\eta_2^{\text{III}}} y^{\text{III}}(\eta^{\text{III}}) d\eta^{\text{III}}. \quad (\text{A15})$$

First we consider the virtual observer in the center ($\chi = 0$). Then we have

$$1 + \bar{z}_1^I = \frac{1}{y^I(\bar{\eta}_1^I)} \quad (\text{A16})$$

$$\frac{1 + \bar{z}_2^{II}}{1 + \bar{z}_1^{II}} = \frac{y^{II}(\bar{\eta}_1)^{II}}{y^{II}(\bar{\eta}_2)^{II}}, \quad (\text{A17})$$

$$\frac{1 + \bar{z}_{\text{rec}}^{III}}{1 + \bar{z}_2^{III}} = \frac{y^{III}(\bar{\eta}_2)^{III}}{y^{III}(\bar{\eta}_{\text{rec}})^{III}}, \quad (\text{A18})$$

where $\bar{\eta}_0^I - \bar{\eta}_1^I = \chi_1^I$ and $\bar{\eta}_2^{II} - \bar{\eta}_1^{II} = \chi_2^{II} - \chi_1^{II}$. Accordingly, we can determine χ_1^I, χ_2^{II} and $\bar{\eta}_{\text{rec}}^{III}$ by specifying his redshifts $\bar{z}_1^I, \bar{z}_2^{II}$ and $\bar{z}_{\text{rec}}^{III}$ ($= 10^3 - 1$), as in Sec. 3.

For an observer at O (with $\eta = \eta_0$ and $\chi = \chi_0$), we obtain

$$1 + z_{\text{rec}}^{III} = \frac{y^{II}(\bar{\eta}_1^{II})y^{III}(\bar{\eta}_2^{III})}{y^I(\bar{\eta}_1^I)y^{II}(\bar{\eta}_2^{II})y^{III}(\bar{\eta}_{\text{rec}}^{III})}, \quad (\text{A19})$$

where $\eta_1^{II}, \eta_2^{II}, \eta_2^{III}$ and η_{rec}^{III} depend on the angle ϕ , contrary to those in Eq. (A18). When we fix $\bar{z}_1^I, \bar{z}_2^{II}$ and $\bar{z}_{\text{rec}}^{III}$ and determine χ_1^I, χ_2^{II} and $\bar{\eta}_{\text{rec}}^{III}$, the final redshift z_{rec}^{III} can be obtained as a function of angle ϕ for $\eta_{\text{rec}}^{III} = \bar{\eta}_{\text{rec}}^{III}$. It is to be noted that η_{rec}^{III} is independent of the existence of the two shells.

B. Models with an intermediate self-similar region

The line-element is expressed in the form (Tomita 1995, 1996)

$$ds^2 = -c^2 dt^2 + S^2(t, r) \left\{ \frac{(1 + rS'/S)^2}{1 - k\alpha(r)r^2} dr^2 + r^2 d\Omega^2 \right\}, \quad (\text{B1})$$

where

$$\alpha(r)/\alpha_0 = 1/(r_1)^2, 1/r^2, \text{ and } 1/(r_2)^2 \quad (\text{B2})$$

for the inner homogeneous region V^I , the self-similar region V^{II} , and the outer homogeneous region V^{III} , respectively, which are shown in Fig. 7. Assuming the matter pressure-free and comoving, the solutions are described using the Tolman solution. The two boundaries $r = r_1$ and r_2 are exactly comoving. The scale factor S in the case $\Lambda = 0$ is given by

$$S/S_0 = \frac{\Omega_0}{2(1 - \Omega_0)} (\cosh \eta - 1), \quad (\text{B3})$$

and

$$\Omega_0 = (cH_0^{-1}/S_0)^3, \quad H_0 \equiv [(\partial S/\partial t)/S]_0. \quad (\text{B4})$$

The time variable t is in the inner, self-similar, and outer regions expressed as

$$H_0 t = \frac{\Omega_0}{2(1 - \Omega_0)^{3/2}} (\sinh \eta - \eta), \quad (\text{B5})$$

$$\xi \equiv \frac{ct}{r} = \frac{c H_0^{-1} (r_1)^{-1} \Omega_0}{2(1 - \Omega_0)^{3/2}} (\sinh \eta - \eta), \quad (\text{B6})$$

$$H_0 t = \frac{r_2}{r_1} \frac{\Omega_0}{[2(1 - \Omega_0)^{3/2}]} (\sinh \eta - \eta). \quad (\text{B7})$$

respectively. The constant α_0 and r_1 are given by

$$\sqrt{\alpha_0} = \frac{4\sqrt{1 - \Omega_0}}{\Omega_0^2 (1 + \bar{z}_1)} \left[1 - \Omega_0 + \frac{\Omega_0}{2} (1 + \bar{z}_1) + \left(\frac{\Omega_0}{2} - 1 \right) \sqrt{1 + \Omega_0 \bar{z}_1} \right]. \quad (\text{B8})$$

and

$$r_1 = [(\Omega_0)^{1/3} / (1 - \Omega_0)^{1/2}] \sqrt{\alpha_0}. \quad (\text{B9})$$

If we define the local Hubble parameter H (in the transverse direction) in the $t = t_0$ hypersurface as

$$H \equiv (\dot{S}/S)_{t=t_0} = [(1/t) \xi S_{,\xi} / S]_{t=t_0}, \quad (\text{B10})$$

H in V^I is equal to H_0 and we have in V^{II} and V^I

$$H t_0 = \frac{\sinh \eta (\sinh \bar{\eta} - \bar{\eta})}{(\cosh \bar{\eta} - 1)^2}, \quad (\text{B11})$$

where $\bar{\eta} \equiv \eta_{t=t_0}$ satisfies

$$H_0 t_0 = \left(\frac{r}{r_1}, \frac{r_2}{r_1} \right) \frac{\Omega_0}{[2(1 - \Omega_0)^{3/2}]} (\sinh \bar{\eta} - \bar{\eta}). \quad (\text{B12})$$

for (V^{II}, V^{III}) , respectively. Present matter densities in the three regions are

$$\rho_{0j} = \frac{3H_0^2 \Omega_0}{8\pi G} \left[1, \frac{1}{3} \left(\frac{r_1}{r} \right)^2 \left(1 - \xi S_{,\xi} / S \right)^{-1}, \left(\frac{r_1}{r_2} \right)^2 \right] \quad (\text{B13})$$

for $j = [I, II, III]$, respectively, and Ω_{0j} is defined as

$$\Omega_{0j} \equiv \rho_{0j}(t_0) / \left(\frac{3H^2}{8\pi G} \right). \quad (\text{B14})$$

The behavior of light rays and redshift formulas were derived in the previous paper (Tomita 1996). If we specify the redshifts \bar{z}_1 , \bar{z}_2 and $\bar{z}_{\text{rec}} (= 10^3 - 1)$, the radii r_1 and r_2 of two boundaries and the value of $\eta_{\text{rec}} (= \bar{\eta}_{\text{rec}})$ are determined, and we can calculate z_{rec} as a function of ϕ , which is the angle between the incident direction and the X axis.

In the following we present additional explanations and corrections for the formulas in the Appendix A of the previous paper(Tomita 1996) : In V^I and V^{III} we have

$$k^r = \pm (S_0/S^2) \{ [1 + \alpha_0(r/r_1)^2] [(w_1)^2 - d^2/(S_0r)^2] \}^{1/2}, \quad (B15)$$

$$k^r = -(S_0/S^2) \{ [1 + \alpha_0(r/r_2)^2] [(w_2)^2 - d^2/(S_0r)^2] \}^{1/2}, \quad (B16)$$

respectively. The second ray in V^I has

$$h_1 = \cosh^{-1} \left\{ \left[1 + (\sqrt{\alpha_0} r_0/r_1)^2 \right]^{1/2} / h_0 \right\} + \{(\eta - \eta_0), -(\eta - 2\eta_m + \eta_0)\} \quad (B17)$$

for $\{\eta \geq \eta_m, \eta \leq \eta_m\}$, respectively. In this paper the incoming angle is

$$\phi = \sin^{-1} \left(\frac{d/w_1}{S_0 r_0} \right) (\equiv \phi_1) \quad \text{and} \quad \pi - \phi_1. \quad (B18)$$

Auxiliary functions V^{III} are expressed as

$$M(\xi) \equiv \frac{1}{N(\xi)} \left\{ (M_0)^2 - 2d^2 \int_{\xi_1}^{\xi} d\xi \frac{N(\xi)}{S^3} \left[SS_{,\xi} + \xi \left(1 + \alpha_0 + SS_{,\xi\xi} - (S_{,\xi})^2 \right) \right] \right\}^{1/2}, \quad (B19)$$

$$\zeta(\xi) \equiv N(\zeta)/[\sqrt{1 + \alpha_0} \xi], \quad (B20)$$

$$\frac{M}{d} = \frac{2(1 - \Omega_0)}{\Omega_0 S_0} \frac{\cosh \eta - 1}{2(1 - \cosh \eta) + \eta \sinh \eta} \left(\frac{M_0}{d} - 2I \right), \quad (B21)$$

and

$$\zeta = \frac{\sqrt{\alpha_0}}{\sqrt{1 + \alpha_0}} \frac{2(1 - \cosh \eta) + \eta \sinh \eta}{(\cosh \eta - 1)(\sinh \eta - \eta)}. \quad (B22)$$

The constants w_1 and w_2 are connected using the junction conditions $(k^0)^I = (k^0)^{II}$ at $r = r_1$ and $(k^0)^{II} = (k^0)^{III}$ at $r = r_2$.

The author thanks N. Sugiyama and N. Sakai for helpful discussions, and a referee for kind comments about past related works. This work was supported by Grant-in Aid for Scientific Research (No. 10640266) from the Ministry of Education, Science, Sports and Culture, Japan.

REFERENCES

Blandford, R. D. and Kundić, T. 1997, The Extragalactic Distance Scale, M. Livio, M. Donahue and N. Panagia, London: Cambridge University Press, 60

Branch, D. 1998, ARA&A, 36, 17

Broadhurst, T. J., Ellis, R. S., Koo, D.C., Szalay, A. S. 1990, Nature, 343, 726

Colless, M. 1995, AJ, 109, 1937

Dale, D. A., Giovanelli, R., and Haynes, M.P. 1999, ApJ, 510, L11

Dressler, A., Faber, S.M., Burstein, D., Davies, R. L., Lynden-Bell, D., Terlevich, R. J., and Wegner, G. 1988, ApJ, 313, L37

Einasto, J. et al. 1997, Nature, 385, 139

Freedman, W. L. 1997, Critical Dialogues in Cosmology, N. Turok, Singapore: World Scientific, 92

Giovanelli, R., Haynes, M. P., Freudling, W., da Costa, L. N., Salzer, J. J., and Wegner, G. 1998, ApJ, 505, L91

Hudson, M. J., Smith, R. J., Lucey, J. R., Schlegel D. J. and Davies, R. L. ApJ, L79; Hudson, M. J., Lucey, J. R., Smith, R. J., and Steel, J. 1997, MNRAS, 291, 488

Humphreys, N. P. et al. 1997, ApJ, 477, 47

Israel, W. 1966, Nuovo Cim. 44b, 1

Kogut, A. et al. 1993, ApJ, 419, 1

Landy, S. D., Shectman, S. A., Lin, H., Kirshner, R. P., Oemler, A., and Tucker, D. 1996, ApJ, 456, L1

Lauer, T. R. and Postman, M. 1994, ApJ, 425, 418; Postman, M. and Lauer, T. R. 1995, ApJ, 440, 28

Lynden-Bell, D., Faber, S. M., Burstein, D., Davies, R. L., Dressler, A., Terlevich, R. J. and Wegner, G. 1988, ApJ, 326, 19

Maeda, K. 1986, Gen. Rel. Grav., 18, 9

Nakao, K., Gouda, N., Chiba, T., Ikeuchi, S., Nakamura, T. and Shibata, M. 1995, ApJ, 453, 541

Riess, A. G., Davis, M., Baker, J., and Kirshner, R. P. 1997, ApJ, 488, L1

Sakai, N., Maeda, K. and Sato, H. 1993, Prog. Theor. Phys., 89, 1193

Sandage, A. and Tammann, G.A. 1997, Critical Dialogues in Cosmology, N. Turok, Singapore: World Scientific, 130

Tomita, K. 1996, ApJ, 461, 507.

Tomita, K. 1995, ApJ, 451, 541; Tomita, K. 1996, ApJ, 464, 1054 for Erratum

Willick, J. A. 1999, ApJ, 522, 647

Zehavi, I., Riess, A. G., Kirshner, P. and Dekel, A. 1998, ApJ, 503, 483

Fig. 1.— A model with a single shell. z and \bar{z} are the redshifts for observers at O and C.

Fig. 2.— A schematic diagram of Hubble and density parameters. A solid and dotted lines denote H_0 and Ω_0 , respectively.

Fig. 3.— Components of the bulk velocity.

Fig. 4.— A diagram for the naive derivation.

Fig. 5.— A model with double shells.

Fig. 6.— A schematic diagram of Hubble and density parameters in a model with double shells. A solid and dotted lines denote H_0 and Ω_0 , respectively.

Fig. 7.— A model with the self-similar region.

Fig. 8.— A schematic diagram of Hubble and density parameters in a model with the self-similar region. A solid and dotted lines denote H_0 and Ω_0 , respectively.

Table 1: Dipole and quadrupole moments and the velocity v_d in the single-shell models.

Ω_0^I	Ω_0^{II}	λ_0^I	λ_0^{II}	h^I	h^{II}/h^I	D ($\times 10^4$)	Q ($\times 10^5$)	v_d (km/sec)
0.2	0.56	0.0	0.0	0.7	0.82	5.56	-2.87	81.8 ¹
0.2	0.88	0.0	0.0	0.7	0.82	8.27	-4.27	121.5 ¹
0.2	0.56	0.0	0.0	0.7	0.90	5.38	-2.79	79.1 ¹
0.2	0.88	0.0	0.0	0.7	0.90	8.21	-4.23	120.7 ¹
0.3	0.56	0.0	0.0	0.7	0.82	3.90	-2.04	57.3 ¹
0.3	0.88	0.0	0.0	0.7	0.82	6.66	-3.39	97.9 ¹
0.2	0.56	0.672	0.430	0.7	0.82	7.92	-3.74	111.4 ¹
0.2	0.56	0.0	0.0	0.7	0.82	5.55	-1.91	81.6 ²
0.2	0.88	0.0	0.0	0.7	0.82	8.21	-2.68	120.7 ²
0.2	0.56	0.0	0.0	0.7	0.82	8.07	-6.35	118.6 ³
0.2	0.88	0.0	0.0	0.7	0.82	12.31	-9.62	181.0 ³
0.2	0.56	0.0	0.0	0.7	0.82	5.57	-2.87	81.8 ⁴
0.2	0.88	0.0	0.0	0.7	0.82	8.27	-4.27	121.6 ⁴

¹ $\bar{z}_1^I = 0.067$, $l_0 = 40(h^I)^{-1}$.

² $\bar{z}_1^I = 0.1$, $l_0 = 40(h^I)^{-1}$.

³ $\bar{z}_1^I = 0.067$, $l_0 = 60(h^I)^{-1}$.

⁴ $\bar{z}_1^I = 0.067$, $l_0 = 40(h^I)^{-1}$, and the shell velocity is 200 km/sec.

Table 2: Dipole and quadrupole moments and the velocity v_d in the double-shell models in the case of $\lambda_0^j = 0$ and $l_0 = 40(h^I)^{-1}$.

Ω_0^I	Ω_0^{II}	Ω_0^{III}	h^I	h^{II}/h^I	h^{III}/h^I	D ($\times 10^4$)	Q ($\times 10^5$)	v_d (km/sec)
0.2	0.36	0.56	0.7	0.92	0.82	5.55	-2.37	81.6 ¹
0.2	0.36	0.56	0.7	0.92	0.82	5.52	-1.44	81.1 ²

¹ $\bar{z}_1^I = 0.067$, $\bar{z}_1^{II} = 0.1$.

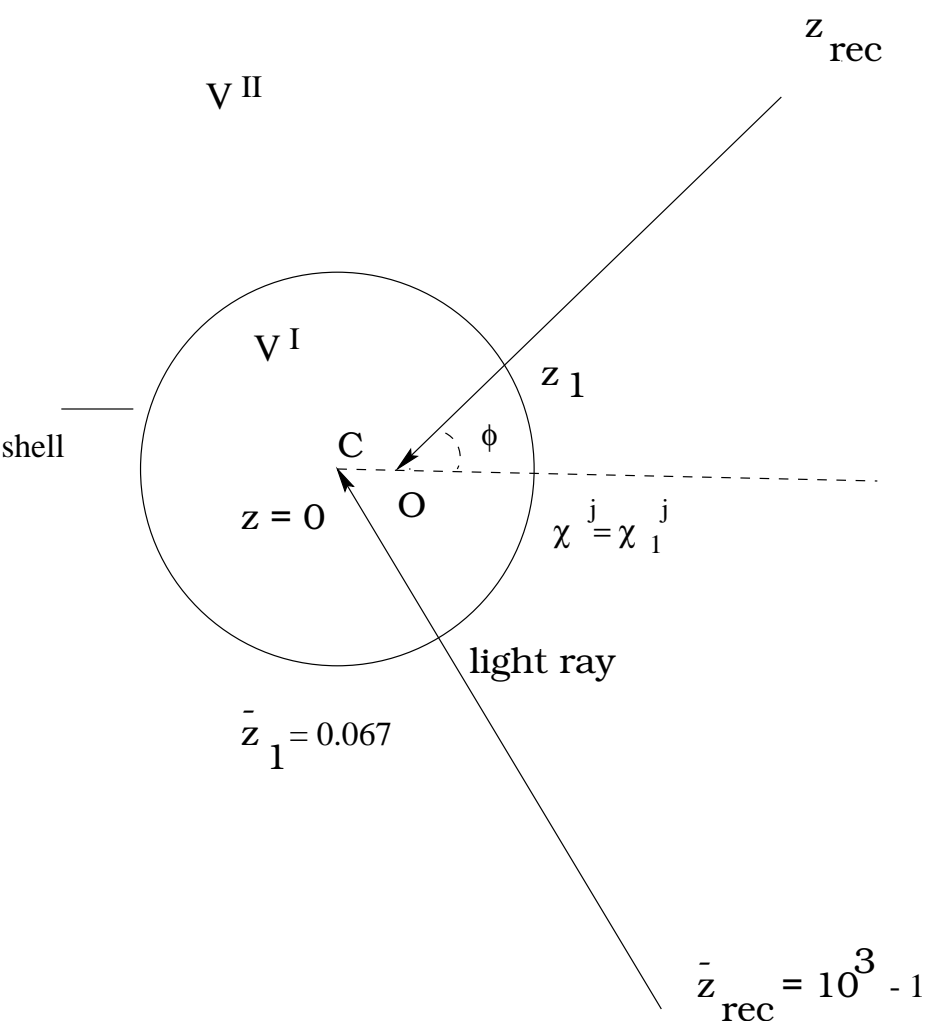
² $\bar{z}_1^I = 0.1$, $\bar{z}_1^{II} = 0.2$.

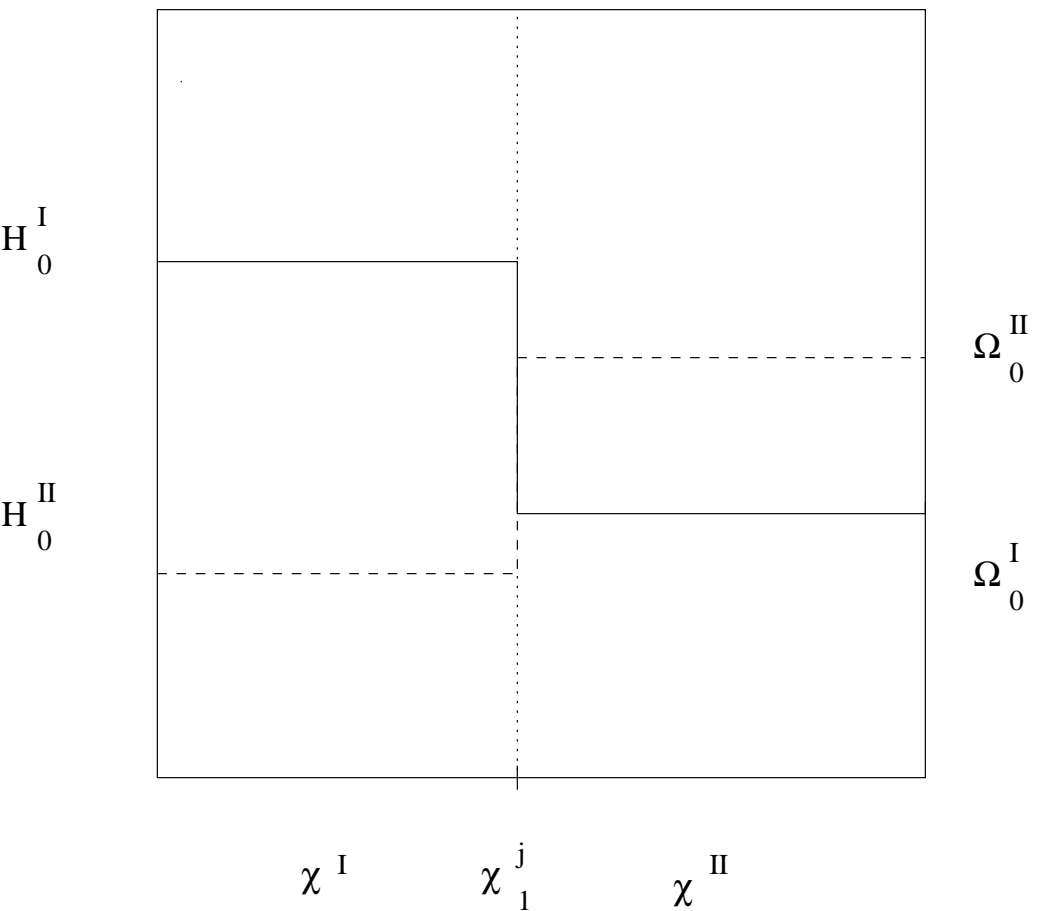
Table 3: Dipole and quadrupole moments and the velocity v_d in the model with a self-similar region in the case of $\lambda_0^j = 0$ and $l_0 = 40(h^I)^{-1}$.

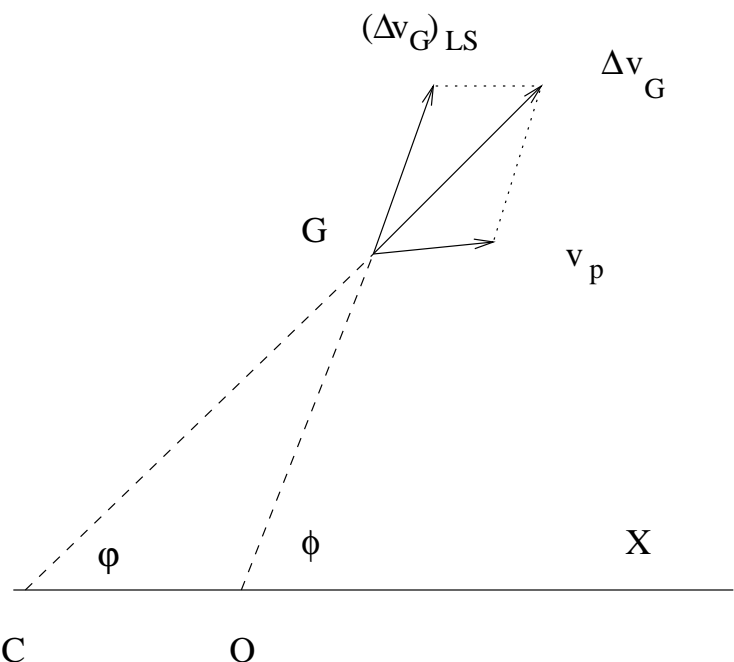
Ω_0^I	Ω_0^{III}	h^I	h^{III}/h^I	D ($\times 10^4$)	Q ($\times 10^5$)	v_d (km/sec)
0.2	0.89	0.7	0.81	8.40	-4.41	123.4 ¹
0.2	0.72	0.7	0.83	7.40	-2.61	108.8 ²
0.3	0.91	0.7	0.84	8.08	-4.11	118.8 ¹
0.3	0.80	0.7	0.86	6.94	-2.25	102.0 ²

¹ $\bar{z}_1^I = 0.067$, $\bar{z}_1^{II} = 0.1$.

² $\bar{z}_1^I = 0.1$, $\bar{z}_1^{II} = 0.2$.







V^{II}

